Floating two-dimensional solid monolayer of C_{60} on graphite

Heekeun Shin,[1] S. E. O'Donnell,[2,*] P. Reinke,[2] N. Ferralis,[3] A. K. Schmid,[4] H. I. Li,[1] A. D. Novaco,[5] L. W. Bruch,[6] and R. D. Diehl[1]

[1]*Department of Physics, Penn State University, University Park, Pennsylvania 16802, USA*
[2]*Department of Materials Science and Engineering, University of Virginia, Charlottesville, Virginia 22904, USA*
[3]*Department of Chemical and Biomolecular Engineering, University of California, Berkeley, California 94720, USA*
[4]*National Center for Electron Microscopy, LBNL, Berkeley, California 94720, USA*
[5]*Department of Physics, Lafayette College, Easton, Pennsylvania 18042, USA*
[6]*Department of Physics, University of Wisconsin, Madison, Wisconsin 53706, USA*

(Received 3 September 2010; published 14 December 2010)

Experiments on both single-crystal graphite and highly oriented pyrolytic graphite indicate that for $60<T<300$ K, C_{60} forms single-layer islands of close-packed molecules at low coverages. Low-energy electron-diffraction measurements on the single crystal indicate that there is almost no preferred orientation of the C_{60} lattice relative to the graphite lattice, producing continuous diffraction rings. A slight preference for the C_{60} lattice oriented at 30° relative to the graphite lattice is explained as originating in the preference for the C_{60} islands to nucleate and align at step edges, observed with scanning tunneling microscopy and low-energy electron microscopy. The energetics of this C_{60} layer were investigated using the Novaco-McTague theory of epitaxial orientation, which found several minimum-energy angles near the experimental C_{60}-C_{60} spacing, inconsistent with the experiment and suggesting an extremely small C_{60}-graphite corrugation. The thermal expansion of this "floating solid" C_{60} lattice for $60<T<120$ K was compared to theoretical models using previously formulated C_{60}-C_{60} pair potentials. The calculated values, assuming perfect two-dimensional layers of spherical C_{60}, are significantly smaller than the measured values, suggesting that additional thermal excitations, such as those involving molecular orientations, are present in this temperature range.

DOI: 10.1103/PhysRevB.82.235427 PACS number(s): 68.35.bp, 68.43.Fg, 68.49.Jk

I. INTRODUCTION

C_{60} adsorbed on graphite represents an interesting case of physical adsorption, where the primary attractive interactions are van der Waals. Although physisorption is generally thought of as a very weak form of adsorption with adsorption energies <0.5 eV, many studies have now been carried out on larger organic molecules which, although their bond to the surface is primarily due to dispersion interactions, have larger adsorption energies that can exceed 1 eV on graphite,[1,2] an energy scale often associated with chemisorption. Due to its size, the C_{60} molecule also has a large van der Waals attraction to graphite, calculated to be nearly 1 eV.[3,4] Although a considerable interest in C_{60} films arises from their use in photovoltaic cells and potential applications in molecular electronics,[5] they are also interesting from a fundamental point of view, as they represent a class of relatively simple model carbon structures. C_{60} adsorption on graphite therefore is a prototypical molecular physisorption system.

There are numerous earlier experimental studies of C_{60} on graphite,[6–16] most of which have addressed the growth of C_{60} on highly oriented pyrolytic graphite (HOPG). The eventual consensus of these studies is that at room temperature, C_{60} grows in a layer-by-layer mode,[7,9,11,12,15] and before the first layer completes, subsequent layers can form dendritic islands that have fractal character.[8,14,16] Since we will later make some comparison to rare gases adsorbed on graphite, it is worth noting that rare-gas adsorption experiments, which typically see the near completion of each layer sequentially,[17] are typically performed in equilibrium with the gas, whereas the C_{60} adsorption experiments are typically non-equilibrium experiments. This difference may affect the nature of the growth.[8] The structures of submonolayer islands were observed in both scanning tunneling microscopy (STM) (Refs. 6, 8, 14, and 15) and low-energy electron diffraction (LEED) (Refs. 7 and 9) to consist of a close-packed arrangement of C_{60} molecules.

A linear-response theory applied to a single C_{60} molecule on graphite found an optimal geometry in which the C_{60} molecule has a hexagonal face down with the C atoms in the bottom hexagonal ring adopting the positions of an additional graphitic layer on top of the substrate, i.e., maintaining the *ABAB* stacking.[3] In this configuration, the binding energy of the C_{60} is 968 meV and the barrier for free rotation of the molecule is 28 meV. The barrier for rotation about the vertical (hex-hex) axis is only a few millielectron volts. The least-favored configuration for the hex-down orientation occurs when the bottom hexagon is above the graphite C atoms (in an *AA* stacking arrangement), with energy 981 meV, giving a lateral energy variation (from highest to lowest potential energy) for the hex-down structure of just 13 meV.

The C_{60}-C_{60} distance from an earlier LEED experiment was 10.5 ± 0.2 Å,[7] and a numerical simulation for a layer of C_{60} on graphite found a C_{60}-C_{60} distance of 9.9 Å.[18] The closest low-order commensurate structure to these is a 4×4 superlattice of the graphite structure, having a nearest-neighbor (NN) spacing of 9.84 Å. Therefore, these results indicate that the C_{60} monolayer is incommensurate or higher-order commensurate. If this is the case, the *ABAB* matching of the C_{60} on graphite found in the Gravil *et al.* calculations for a single molecule[3] will not be maintained across the monolayer. The earlier STM observations indicate a rather

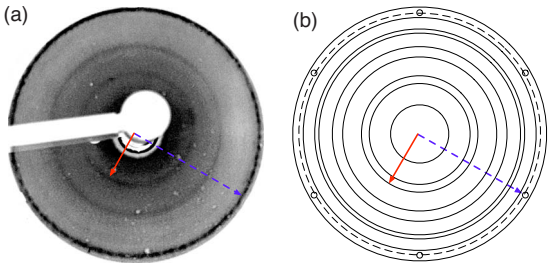

FIG. 1. (Color online) LEED pattern (inverted intensity) from a monolayer film of C_{60} on HOPG at $T=100$ K and $E=70$ eV. The outer (dark) ring is the first-order diffraction from the HOPG. The arrows point to the third-order C_{60} ring (solid) and the first-order graphite ring (dashed). (b) Schematic of the diffraction rings from the C_{60} monolayer. The solid rings correspond to the close-packed C_{60} structure and the dashed ring indicates the location of the HOPG first-order diffraction ring. The small circles indicate where diffraction spots would occur from SCG.

uniform monolayer structure, i.e., no sharp domain walls (density modulations), consistent with a small C_{60}-graphite corrugation, and raising the possibility that this incommensurate monolayer could exhibit a Novaco-McTague (NM) (Refs. 19 and 20) epitaxial lattice alignment, similar to those observed for rare gases on graphite.[17]

The NM theory of orientational epitaxy, based on the elastic response of the overlayer to the substrate potential, predicts the equilibrium orientational alignment of an incommensurate overlayer lattice. In such an overlayer, the molecules experience competing adatom-adatom and adatom-substrate lateral forces, and in general, the overlayer lattice in equilibrium will not align along a symmetry direction of the substrate. The NM theory correctly predicted nonsymmetry overlayer lattice alignments in various types of monolayers, e.g., for rare gases on graphite,[21] and recently has also been applied to a monolayer of C_{60} on Pb(111).[22] The C_{60}-graphite lattice alignment was not determined in earlier experiments because of the difficulty for STM to resolve atomic structures in both the monolayer and the substrate at the same time (discussed below), and because there have been no diffraction experiments for C_{60} adsorption on single-crystal graphite (SCG).

The LEED experiments presented here were carried out on SCG to study the orientational epitaxy of the C_{60} monolayer and on HOPG in order to provide a comparison to the other experiments that used HOPG. In order to gain a more microscopic understanding of the LEED results, STM experiments were performed to image both the graphite and C_{60} lattices, providing a local-order measure of the orientational epitaxy. Because surface defects (steps) were observed to be involved in the growth of C_{60}, low-energy electron microscopy (LEEM) measurements were used to observe the growth over a wider field in real time. Surprisingly, the LEED results on SCG indicate almost no preference for the epitaxial angle of the C_{60} lattice. This is highly unusual, never having been observed for any monolayer on graphite, or for C_{60} adsorbed on any surface. A similar lack of preference for lattice orientation may exist for rare gases on some metal surfaces, e.g., metastable rings were observed in diffraction patterns from Xe on Ag(111),[23] but the presence of surface steps seems to exert a dominant aligning influence in all known cases.[1,17] The apparently truly incommensurate "floating monolayer"[24] of C_{60} on graphite observed here was analyzed using Novaco-McTague theory, and measurements of its two-dimensional (2D) thermal expansion were compared to model calculations using two commonly used C_{60}-C_{60} potential models.

This paper is organized as follows. The procedures followed in the LEED, STM, and LEEM experiments are described, followed by the experimental LEED results concerning the structure and orientation of the C_{60} monolayer. Then a Novaco-McTague analysis of the epitaxial orientation of a monolayer of C_{60} on graphite is presented. This is followed by STM and LEEM results for the growth of C_{60} on graphite. Finally, some simple modeling results for the lattice constant and thermal expansion of the overlayer are presented and compared to the experimental results.

II. EXPERIMENTAL PROCEDURES

The LEED experiments[25] were performed at Penn State, the STM experiments[16] were performed at University of Virginia, and the LEEM experiments[26] were performed at Lawrence Berkeley Laboratory. The LEED experiments were performed with both SCG and HOPG substrates; the STM and LEEM experiments used HOPG. The adsorption studies were carried out in ultrahigh vacuum, and in all cases, the graphite was annealed for several minutes to at least 300 °C to drive-off residual impurities. The C_{60} films were sublimed C_{60} from a crucible that contained 99.95+% pure C_{60} powder, and the deposition rate was controlled by adjusting the source temperature. In preparation for the LEED experiments, the sample temperature was typically held at 377 K during dosing to achieve a monolayer, but a single layer of C_{60} could also be achieved by dosing for longer with the sample held at 490 K. In the STM experiments, there was no difference observed in submonolayer lattice structures for dosing at room temperature and for dosing at (or heating to) a higher temperature. The presence of the second layer was detected in the LEED by the observation of additional half-order rings at low temperature. The transition between this double-period superlattice phase and the 1×1 structure was observed to occur at about 230 K, as observed in earlier experiments for C_{60} on HOPG.[7] In STM and LEEM, the onset of the second-layer growth could be directly observed, of course. We note that in both STM and LEEM, the growth of the second-layer islands was observed to begin before the completion of the monolayer, i.e., second-layer islands form on top of first-layer islands, which implies that the LEED data were obtained for coverages well below one monolayer. The LEED data were acquired and analyzed using a home-built data acquisition system[27] while image analysis of the STM data was performed using the WSXM (Ref. 28) and SCALA software packages.

III. ORIENTATIONAL ALIGNMENT OF C_{60} Lattice

A. LEED measurements

An earlier comparative LEED study of clean SCG and HOPG surfaces demonstrated that SCG produces the diffrac-

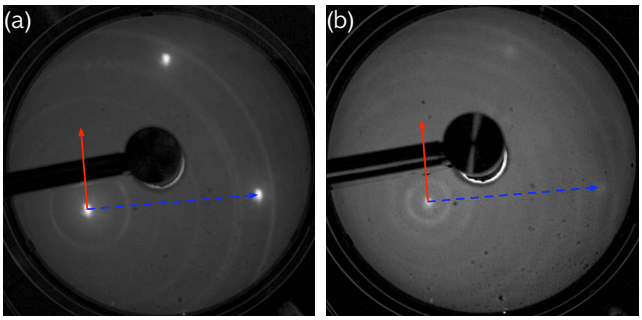

FIG. 2. (Color online) Two LEED patterns for C_{60} on high-quality SCG for (a) a submonolayer at an electron-beam energy of 60 eV and a sample $T=62$ K, and (b) a bilayer C_{60} at an electron beam energy of 61 eV and 120 K. The specular beam is the bright spot below and to the lower left of the center and first-order graphite spots are visible at the top and right of the pattern. These spots are large in (a) due to overexposure. The arrows correspond to the same diffraction features as for Fig. 1.

tion pattern expected for a hexagonal structure, whereas HOPG, which consists of many crystallites having random in-plane orientations, produces a pattern with diffraction rings.[25] Aside from the crystallite size and orientational alignment, however, there is no difference in the atomic-level graphite structure.[25] Figure 1 shows the normal-incidence LEED pattern from C_{60} on HOPG for incident beam energy of 70 eV. In this pattern, the first-order diffraction ring from the HOPG is near the edge of the screen. Although it is not readily visible in Fig. 1, this ring can be seen to be composed of discrete spots that come from distinct graphite crystallites. The rings inside the graphite ring are due to the ordering of C_{60}. These do not show evidence of discrete spots, indicating that the domain size of the C_{60} is smaller than that of the graphite. The relative diameters of the rings are consistent with those expected from a hexagonal lattice, as found in the earlier LEED study of C_{60} adsorption on HOPG.[7]

Figure 2 shows two off-normal incidence diffraction patterns for submonolayer and bilayer C_{60} adsorbed on SCG. Surprisingly, the C_{60} produces diffraction rings rather than spots, indicating that there is no clear preference for epitaxial orientation of the C_{60} lattice on the graphite lattice. The rings are sharper in the radial direction than those observed on HOPG, consistent with the out-of-plane mosaic spread being smaller than for HOPG. The lack of structure within the rings indicates that there are many microcrystallites (>150 Å in extent) having almost random orientations within the part of the sample illuminated by the electron beam, which is about 0.25 mm in diameter. The C_{60}-C_{60} spacing obtained from the diffraction rings is 9.987 ± 0.006 Å for $T=120$ K, using the proximate graphite diffraction spots as fiducial points. In the bilayer pattern, additional rings are present due to the doubling of the structural period of C_{60} in the orientationally ordered film.[7]

Although the diffraction rings from the C_{60} overlayers are continuous, they are not completely isotropic. Figure 3 shows an analysis of the azimuthal intensity of the diffraction rings from the monolayer C_{60} diffraction pattern. In Fig. 3(a), the bright spot in the upper left is the (0 0) beam and two bright spots in lower section are first-order graphite diffraction spots. Figure 3(b) shows the intensity profile along the azimuthal curves shown by dotted arcs in Fig. 3(a), one through the graphite spots and one through the first-order C_{60} diffraction ring. From these profiles, we can see that the C_{60} layer has a slight preference for the orientation of 30° relative to the graphite orientation, although the C_{60} peaks are very broad as indicated by the Gaussian fit parameters to these peaks given in Fig. 3(c). The full width at half maximum of the C_{60} peaks is almost 30°, a reflection of how weak the preference is for the 30° orientation. It was also observed in these experiments that different graphite crystals

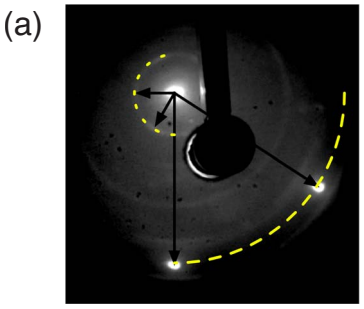

(b)

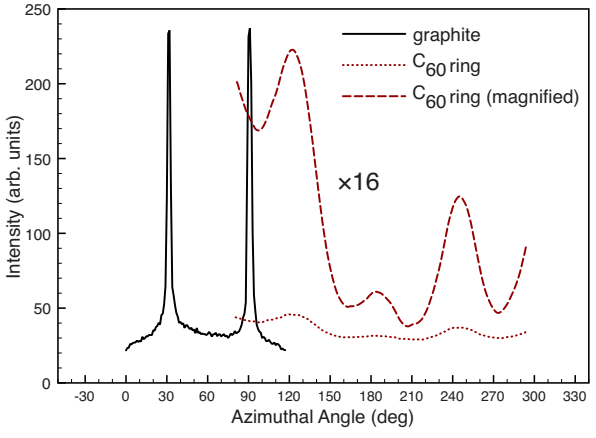

(c)

	Peak angle	FWHM
SCG	30.3 ± 0.1°	4.7 ± 0.1°
	89.5 ± 0.1°	4.7 ± 0.1°
C_{60}	123.0 ± 1.0°	31.3 ± 0.1°
	185.0 ± 0.1°	22.8 ± 0.3°
	243.0 ± 1.0°	27.4 ± 0.1°

FIG. 3. (Color online) (a) LEED pattern from C_{60} on SCG ($E=58$ eV, $T=120$ K). The arrows indicate the k-space unit-cell vectors for the graphite, and the 30° direction vectors for the C_{60} ring. The dashed arcs show the locations for the azimuthal profiles shown in (b). Their origin is at the position of the specular beam (tails of arrows). (b) The azimuthal intensity profiles from the LEED pattern shown in (a), indicating maxima for the inner C_{60} ring along directions 30° from the graphite directions. The angle scale on the profiles starts from the positive x axis of the pattern in (a) and increases in the clockwise direction. (c) Gaussian parameters from fits to the azimuthal profile peaks shown in Fig. 3(b). The slight offset of the centers of the peaks from the 30° symmetry directions is due to the slight distortion in the LEED pattern from being at non-normal incidence.

produced more or less preferential alignment along the 30° direction, depending on crystal quality, but in all cases, the diffraction rings were continuous. This will be discussed later in Sec. III C.

B. Novaco-McTague analysis

It is clear from the continuous diffraction rings that there is not a strong preference for orientational alignment of the C_{60} lattice, which differs from other physisorbed monolayers on graphite. For incommensurate rare gases on graphite in particular, the equilibrium epitaxial angles were observed to vary with lattice parameter, and their dependence was well described by the NM theory,[19,20] which treats the relaxation of an elastic overlayer in response to an incommensurate substrate potential. The resulting epitaxial angle depends on both the overlayer-overlayer and overlayer-substrate interactions.

The calculations here used a fully nonlinear mass density wave expansion in the quasiharmonic approximation.[29] A simple version of this theory has been published for Xe on graphite.[30] The interactions were based on the self-consistent C_{60}-graphite potential by Gravil[3] and the spherically averaged Girifalco C_{60}-C_{60} potential.[31] Three Fourier amplitudes were used to model the potential in the contour plots shown in Fig. 2 of Gravil *et al.*[3] The radius of the spheres in the Girifalco potential was reduced by 0.02 Å to give the same lattice spacing as determined experimentally at 120 K (9.99 Å). For this lattice spacing, there are three distinct angles for which the mass density wave energy decreases by about 0.6 meV, namely, 0°, 8°, and 29.9° relative to the graphite lattice, plus the symmetric angles about the 0° axis. Although multiple minima typically did not occur in NM calculations for rare-gas monolayers,[19] they did occur for C_{60} on Pb(111).[22] This is because the larger ratios of lattice spacings of the overlayer and substrate produce more nearby significant higher-order commensurate matches.

The situation for C_{60} on graphite was explored further by calculating the equilibrium angle as a function of the C_{60} lattice parameter. A strong dependence of the angle on lattice parameter was observed near the experimental lattice parameter. The optimal angle changed from near 30° for a slight (~0.1%) expansion of the lattice to 8° and then to 0° for a slight (~0.2%) compression, consistent with the multiple energy minima observed at the experimental lattice parameter. Because the relative energies of the different lattice angles depend on the exact potential parameters used in the calculation, it is difficult to make a precise prediction, but the expectation is that multiple angles would be observed at the experimental lattice parameter. This may be consistent with the experimental observation, which shows a continuous distribution of angles, although, in light of the observations for C_{60} on Pb(111), where distinct angles were observed in coexistence,[22] it seems more likely that the continuous distribution of angles is due to an extremely weak orienting force. This suggests a very small potential-energy corrugation relative to the C_{60} monolayer elastic energy. This will be discussed in Sec. V.

The LEED experiments on SCG show a continuous distribution of angles with a slight maximum in the diffraction ring intensity in the direction 30° from the graphite lattice, shown in Fig. 3. This could be a manifestation of the NM effect, but since surface defects such as steps can dominate the orientations of adsorbed films,[32] we have investigated the effect of steps for C_{60} on graphite using STM and LEEM, as described in Sec. III C.

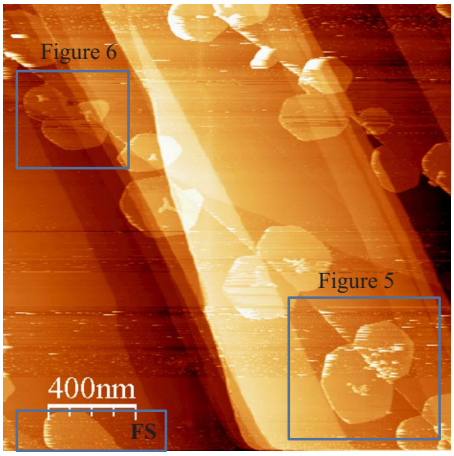

FIG. 4. (Color online) STM image showing C_{60} monolayer islands in the vicinity of a graphite step edge. While most islands are attached to the step, one free-standing island can be observed at the lower left (FS). Details of two marked sections are shown in Figs. 5 and 6. All STM data were acquired at room temperature.

C. LEEM and STM Measurements

Using STM, we investigated the relative alignment of the C_{60} and graphite lattices, and whether the steps or edges exert an orientational alignment on the C_{60} monolayer islands. Because of the large difference in heights and electronic structures of the C_{60} molecules and the graphite substrate, each measurement required separate scans to image their respective lattices. The imaging conditions that yield atomic resolution with an etched W tip are a tunneling current of 0.27 nA and a bias voltage of 0.125–0.25 V for graphite, and a lower current of 0.09 nA and a higher voltage of 1.8 V for the C_{60}. Since C_{60} is a semiconductor with a gap of about 2.3 V, it does not have electronic states available for tunneling at low-bias voltages and only the underlying HOPG substrate is imaged. This usually leads to destruction of the C_{60} layer and prohibits simultaneous imaging of both C_{60} and graphite. Therefore the C_{60} islands were imaged first and then an adjacent area of graphite.

At submonolayer coverages on HOPG, C_{60} forms monolayer islands, which almost exclusively nucleate and grow from step or domain edges. This can be seen clearly in the STM image in Fig. 4, which shows numerous C_{60} islands attached to step edges and one free-standing island at the lower left corner of the image. This propensity for growth at step edges is undoubtedly related to the high mobility of the C_{60} on the graphite surface. The average distance that C_{60} molecules diffuse before joining an island was determined to be about 300–400 nm in an earlier experiment that observed the growth of C_{60} islands on graphite with arrays of artificial nucleation sites.[33,34]

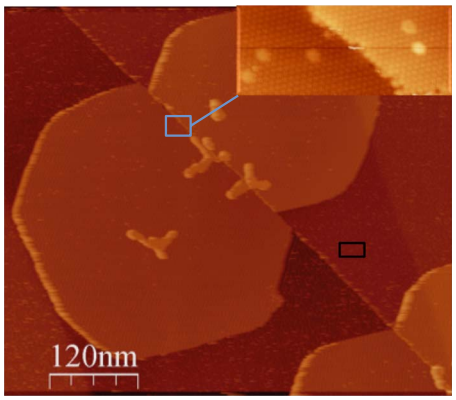

FIG. 5. (Color online) Two of the islands shown in the lower right-hand corner of Fig. 4. The inset shows a high-resolution scan of the area indicated by the square. The other (black) box is the area where the graphite lattice was imaged.

In Fig. 4, several lines transect the image. These are step edges, edges of graphite flakes that are folded, and depressions in the graphite surface probably caused by mechanical deformation during sample preparation. These structures can be seen more clearly in Figs. 5 and 6, where the areas marked by the squares are shown in detail. The true step edges are distinguished by their characteristic height, and they appear slightly smudged in the STM images due to the accumulation of trapped molecules not yet incorporated into islands and which are mobile under the influence of the STM tip. We consider the following three representative image sections: (1) a single free-standing fullerene island, (2) two islands on either side of a graphite step edge, and (3) a complex arrangement of several islands on either side of a graphite step edge, which includes a graphite depression line and a low-angle grain boundary. The small fractal or triangular structures that are visible on some of the islands are the

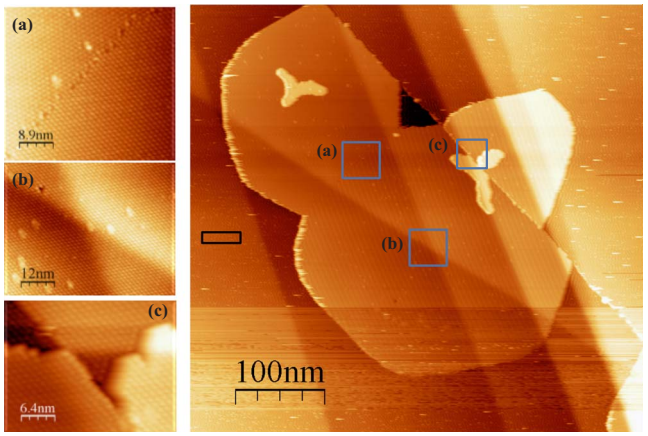

FIG. 6. (Color online) Three of the islands shown in the upper left hand corner of Fig. 4. High-resolution scans are shown on the left for the three areas indicated on the right. (a) shows a grain boundary within the fullerene monolayer. (b) corresponds to an area where the fullerene layer covers a depression in the graphite and not a step edge. (c) shows an area that includes the second-layer dendrites. The other (black) box is the area where the graphite lattice was imaged.

second layer of fullerenes. Their shape has been studied in detail earlier.[8,16]

The islands shown in Figs. 5 and 6 provide representative examples of the STM observations of the lattice orientation of the C_{60} islands at step edges. These islands are all adjacent to the same step edge with identical orientation of the graphite lattice on either side of the step edge. In Fig. 5, the orientations of the fullerene islands on either side of the step edge are identical and both are rotated by 20° with respect to the graphite lattice (measured from Fourier transforms of the images). Figure 6 shows three connected islands. The bottom island and the small one on the opposite side of the step have the same lattice orientation as each other (c). The large island on the left includes a 10° grain boundary (a), where two nearly equal size islands are connected. In the free-standing island (labeled FS in Fig. 4), the C_{60} lattice is rotated by 20° relative to the graphite lattice. The error in the angle measurements of the respective C_{60} and graphite lattices can be as much as 15° in some cases due to the need to move to a slightly different location, which introduces some image distortion due to the nonlinearity of the piezoceramic elements.

These experiments are sufficiently time consuming that a large number of scans was not feasible. Instead, 10–15 images were measured to look for evidence of the correlations of the C_{60} lattice relative to the graphite lattice and relative to the step edges, if present. In these measurements, no correlation was observed for the relative orientation of the C_{60} lattice to the graphite lattice. However, a slight preference was observed for an alignment of the C_{60} lattice relative to the step edges, in which the close-packed C_{60} rows preferentially align along the step edges. Therefore, we conclude that the C_{60} islands that grow from step edges, which are the majority of islands on HOPG, have a preference for alignment of close-packed C_{60} rows along the step edges. In LEED, this preferential alignment would not be observed because of the random orientation of graphite crystallites, but it would be observed on SCG if the step-edge direction is uniform.

On HOPG, there appears to be little correlation between the graphite lattice and the direction of step edges. On SCG, however, the step edges and domain boundaries tend to be long, straight and along the $\langle 1\bar{1}00\rangle$ symmetry directions of the graphite,[35,36] which correspond to the 30° direction. This is a key to understanding why we see a preference for the alignment of C_{60} on SCG: a preference for the 30° C_{60} lattice alignment along these step edges will lead to more scattering along the 30° direction in the LEED patterns from C_{60} on SCG. We note that a relatively stronger diffraction signal at 30° was observed on lower-quality SCG crystals, which likely have a higher step density.

The importance of diffusion and step-edge nucleation on the growth was also observed in LEEM images, shown in Fig. 7. LEEM provides a broader view of the growth and shows how growth along step edges dominates the growth of the monolayer on HOPG.

IV. LATTICE CONSTANT AND THERMAL EXPANSION

The present experiments show that the C_{60} monolayer does not form a commensurate or high-order commensurate

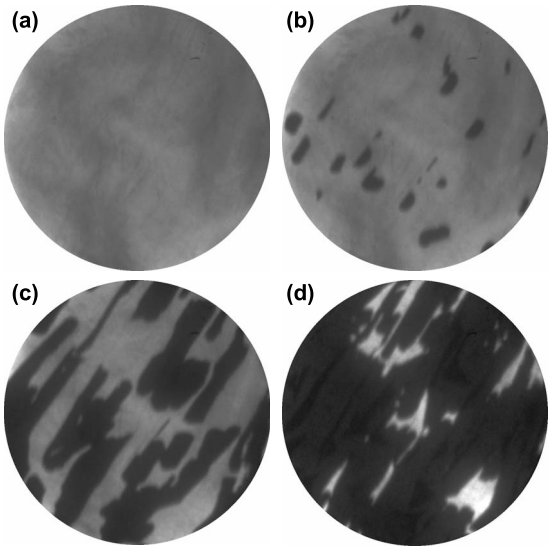

FIG. 7. Successive LEEM images (field of view is 5 μm diameter, lateral resolution is 10 nm, vertical resolution is <0.1 nm, and typical terrace width is about 0.1 μm) during adsorption a monolayer of C_{60} on HOPG at 408 K. (a) Clean HOPG, the primary step or domain edges can be seen faintly running approximately southwest (SW) to northeast (NE). [(b)–(d)] The growth of the C_{60} monolayer is mainly along the step edges. Relative dosing times are (a) 0, (b) 0.04, (c) 0.58, and (d) 1. All LEEM data were acquired with a primary beam energy of 11 eV.

lattice on graphite and that its orientation relative to the graphite has a very broad distribution. We infer that the C_{60}-graphite interaction is flat. Therefore the C_{60} monolayer is a good candidate to be a floating 2D solid.[24] We test this hypothesis with measurements of the monolayer thermal expansion and with comparative modeling of the lattice constant and thermal expansion of the monolayer and three-dimensional (3D) C_{60} solids.

A. Measurements

We determined the thermal expansion of the monolayer by directly measuring the lattice parameters from the LEED patterns. The value for the linear-expansion coefficient is $100 \pm 30 \times 10^{-6}$ K^{-1} for $60 < T < 120$ K. These measurements were performed at relatively low temperatures because the thermal scattering at higher temperatures made the measurements less precise. Even at the temperatures measured, the measurement is imprecise using LEED. This is because it is most accurate to measure both a substrate peak and an overlayer peak simultaneously, and due to the variation in their intensities with the beam energy, this is quite difficult to achieve for this system.

This value for the monolayer thermal expansion and previous experimental and theoretical results for the thermal expansion of 3D solid C_{60} are assembled in Table I. There is an orientational ordering transition in the 3D solid at about 255 K, above which the C_{60} molecules are orientationally disordered, and below which they are orientationally ordered in a superlattice having twice the C_{60}-C_{60} spacing. For the monolayer on graphite, there is no evidence of superlattice formation down to 60 K. One possible explanation is that the substrate exerts a sufficient preference for one orientation of the C_{60} (e.g., the hexagon down is preferred and the barrier to rotation is 28 meV according to one calculation[3]) that it prevents the formation of the favored C-C bond—pentagon configuration that is believed to drive the bulk phase transition due to its higher packing efficiency.[37]

The values measured for thin films increase with decreasing thickness, as shown in Table I, with a value of 44×10^{-6} K^{-1} obtained for a film having a thickness of about four layers. At this thickness, the film already exhibits the superlattice transition that results in orientational order and a jump in density at the transition. The value obtained for a monolayer is more than twice that, which seems very large compared to the prediction, but might be feasible if the monolayer also undergoes some degree of orientational ordering (continuously, without a superlattice) over the temperature range of the measurement. We note that for the 3D case, the experimental measurements show strong variations in the thermal-expansion coefficient with temperature *below* the orientational ordering transition, where there is still significant librational motion.[39,40]

B. Modeling

In order to draw a comparison of the earlier 3D studies and our monolayer study, we have calculated the lattice constants and the thermal expansion of both 3D C_{60} and the C_{60} submonolayer using quasiharmonic theory (QHT) and classical cell model calculations.[42] QHT denotes results based on a calculation of the Helmholtz free energy in the harmonic lattice approximation with force constants that depend on the lattice spacing. The classical cell model calculations evaluate the free energy in a single-particle approximation in which the cell free area or free volume is evaluated for the C_{60} moving in the field of its fixed neighbors. The cell model includes more effects of the anharmonicity of the motions and for the rare-gas solids is found to be more reliable than the QHT approximation at intermediate temperatures that are still below the melting temperature.[43,44] We checked the 2D cell model calculation for C_{60} near 100 K with a self-consistent phonon approximation[30] and found agreement to about 5% with the value in Table I.

The calculations here employed two different models for the C_{60}-C_{60} potential: the spherically averaged potential of Girifalco[31] used for the NM calculations and the first-principles calculation by Pacheco and Prates Ramalho.[45] From a practical point of view, the main difference between the two potential models is that the Girifalco has a steeper rise in potential energy at close range, leading to a stiffer close-range interaction, as seen in Fig. 8. Figure 8 shows a comparison of the calculated C_{60}-C_{60} potentials with a Lennard-Jones (L-J) 12-6 potential, scaled to have the same well depth and interaction length as the C_{60} potentials. The C_{60} potentials are considerably narrower than the L-J potential, indicating a more rigid lattice relative to the interaction strength.

The calculations were performed for both 2D and 3D structures, using potential energy sums to five shells of

TABLE I. Calculated and experimental values for the linear coefficient of expansion α in the stated temperature interval. QHT refers to the quasiharmonic theory results.

3D theory	α ($\times 10^{-6}$ K^{-1})	T interval (K)
QHT with atomic/bond pairwise 12-6 potentials +electrostatic interaction[a]	26	270–330
QHT with atomic exp-6 potentials and Euler angles for librations[b]	16	$T>100$
Classical cell model (spherical C_{60} potentials) (this study)	8	50–200
3D experiment		
Neutron diffraction[c]	17	260–320
X-ray diffraction and neutron diffraction[d]	21	260–320
2D theory		
Classical cell model (spherical C_{60} potentials) (this study)	14–15	60–120
QHT (spherical C_{60} potentials) (this study)	18	60–120
2D and thin-film experiment		
10 nm thick—dilatometry[e]	27	80–260
4.5 nm thick (~10 layers)—dilatometry[e]	36	80–260
3.5 nm thick (~4 layers)—dilatometry[e]	44	80–260
Monolayer—LEED (this study)	100 ± 30	60–120

[a]Reference 37.
[b]Reference 38.
[c]Reference 39.
[d]Reference 40.
[e]Reference 41.

neighbors. The Einstein frequency for both models is about 40 K, and the de Boer parameter is about 0.003, implying that the system is essentially classical in the temperature range of the experiments, 60–120 K. The cell potential circular or spherical average used three shells of neighbors. The nearest-neighbor distances obtained are shown in Table II and the thermal-expansion results are in Table I.

From Table II we can see that the difference in NN distance between the cell model and QHT in 2D is about 0.04% at 100 K, which is negligible for the discussion of the experimental lattice constants. If we use the cell model to compare the difference between 2D and 3D, we find that the ratio $L(2D)/L(3D)=1.001$ at 0 K and 1.0021 and 1.0026 at 100 K, for the Girifalco and Pacheco potentials, respectively. The corresponding ratio of the experimental values is 1.005. These values indicate that for both models, the calculations give results consistent with the experiments for the change from 2D to 3D. This ratio is distinctly smaller than a corresponding experimental values 1.01–1.02 for Kr/Ag(111) and Xe/Ag(111), which are considered to be prototypical floating monolayer solids.[46,47] The difference can be understood from the comparison of potentials in Fig. 8, which show that the C_{60} potentials are more concentrated at the nearest-neighbor distance compared to the L-J potential that is a generic model for rare gases.

The classical cell model gives a nearly linear lattice constant vs temperature from 50 to 400 K whereas the QHT becomes supralinear above about 200 K. Similar dependencies have been found for rare gases.[43,44] Table I shows the

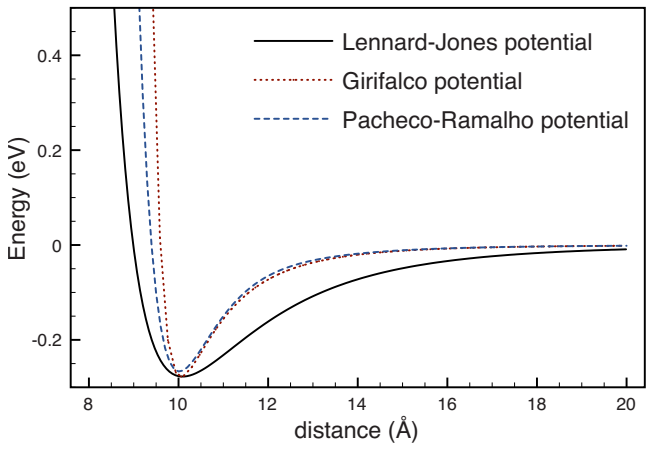

FIG. 8. (Color online) Girifalco and Pacheco-Ramalho C_{60}-C_{60} potentials, and a L-J 12-6 potential scaled to the same well depth and interaction length as the C_{60} potentials.

TABLE II. Results of the cell model and QHT calculations for potential energy and NN distance in 2D and 3D. Lengths L are at the minimum of free energy. Potential energy sums per molecule include five shells of neighbors. The cell potential spherical/circular average includes three shells of neighbors. Experimental NN for 2D and 3D are 9.99 Å (this study) and 9.94 Å (Ref. 39), respectively.

	Girifalco	Pacheco
Pair potential min ε at	277 meV	267 meV
R_{min}	10.056 Å	10.018 Å
3D cell		
Static potential min (0 K)	1787 meV	1719 meV
at L=	10.042 Å	9.999 Å
NN (100 K)	10.045 Å	10.003 Å
2D cell		
Static potential min (0 K)	851 meV	819 meV
at L=	10.052 Å	10.012 Å
NN (100 K)	10.066 Å	10.026 Å
NN (120 K)	10.069 Å	10.029 Å
2D QHT		
NN (100 K)	10.070 Å	10.030 Å
NN (120 K)	10.073 Å	10.034 Å

thermal-expansion coefficients derived using QHT and the classical cell model for 2D C_{60} in the temperature range of the experiments. The cell model 3D values calculated in this study, also in Table I, are somewhat smaller than the 2D values, consistent with the lattice constant values presented in Table II.

The 3D values calculated in this study are smaller than those from earlier calculations (Table I). The 3D QHT value from calculations that use atomistic potentials and molecular librations is somewhat larger (16×10^{-6} K^{-1}), and the result from calculations that employ the additional electrostatic terms is even larger (26×10^{-6} K^{-1}). The experimentally measured values are between these latter two values. It appears that the inclusion of the rotational degrees of freedom has a significant effect on the thermal-expansion coefficient, which may be related to the possibility of more efficient packing available to stationary molecules compared to rotating molecules. Since there are no other predictions of the thermal-expansion coefficient for 2D C_{60}, we estimate what an atomistic model might give by the ratio of the 2D and 3D cell model values. The result is an estimate for the monolayer in the range 30×10^{-6}–49×10^{-6} K^{-1}. This is comparable to the thermal expansion of the four-layer film, Table I, but only half of the value in our experiments. Therefore, it would be beneficial to have additional experimental determinations of this value as well as simulations using atomistic potentials.

V. DISCUSSION

Combining the LEED, STM, and LEEM results, we conclude that the C_{60}-graphite lateral interaction is so weak that it does not exert a sufficient orienting force to align a large C_{60} domain in any particular direction at the temperatures that have been studied. We attribute a weak preference for the 30° orientation to the alignment effect of step edges, a conclusion which is supported by the STM observations of islands near step edges and on the variability of the extent of alignment with SCG perfection (not shown here). On SCG, step free regions can be hundreds of microns in extent,[48] about 100–1000 times the typical terrace sizes on HOPG (see Fig. 7). Therefore, the relative effect of orienting forces exerted by the steps is expected to be considerably less for submonolayer islands on SCG, and so the corrugation of the C_{60}-graphite potential should provide the dominant orienting force.

It is interesting to compare C_{60} and rare gases adsorbed on graphite further. Ne, Ar, Kr, and Xe all form incommensurate structures on graphite under the appropriate conditions, and each of them displays a variation in epitaxial angle with lattice spacing that implies an epitaxial aligning force such as that described by the NM theory. Table III lists the dimer potential well depth, the adsorbate-graphite corrugation (calculated for Xe and Ar using DFT and deduced from the zone-center gap of the in-plane vibration frequency for Kr), and the calculated NM energy. The NM energy is the energy of the adlayer modulation driven by the substrate corrugation and its variation with angle drives a rotation of the adlayer relative to the substrate. The calculated NM energy is significantly larger for C_{60} than for the rare gases. This arises from the larger corrugation energy but is partially offset by the greater stiffness of the adlayer response, reflected in Fig. 8.

The lack of a preferred orientation observed in the C_{60} experiments suggests that the corrugation is effectively zero or alternatively that the lateral extent of the islands is not sufficient to sustain a rotation relative to the steps. The latter explanation seems less likely, since the epitaxial rotations observed for Ar and Kr on graphite were observed at submonolayer coverages where the island would be expected to have a similar extent as the C_{60} islands studied here. Although the calculated potential-energy variation for a C_{60} molecule adsorbed with its hexagonal face down is 13 meV [compared to an adsorption energy of 968 meV (Ref. 3) and a C_{60}-C_{60} interaction energy of about 278 meV (Ref. 31)], this is for a molecule that is translated rigidly across the surface. In reality, the molecules are likely to be spinning in the temperature range of interest (the calculated barrier to rotation about the hexagonal face axis is just a few millielectron volts[3]) and will also experience vibrations and librations at finite temperatures. Thermal motion was not considered in the NM calculations presented here and would be expected to reduce the effective substrate corrugation.[30] Thus, the large size and additional molecular degrees of freedom of

TABLE III. Dimer well depths D, adsorbate-graphite corrugation energies ΔV, and NM energies E_{NM}. Energies are in millielectron volt. The calculations are for triangular lattices with nearest-neighbor spacings (in Å) 3.12, 3.816, 4.041, 4.546, and 9.987 for Ne, Ar, Kr, Xe, and C_{60}, respectively.

Adsorbate	D	ΔV [a]	ΔV(NM) [b]	$\Delta V(CC)$ [c]	$E_{NM}(\Delta V)$ [d]	$E_{NM}(VCC)$ [e]
Ne	3.65 (Ref. 1)		2.91	3.71		−0.072
Ar	12.3 (Ref. 1)	9.0 (Ref. 1)	3.58	5.37	−0.374	−0.133
Kr	17.1 (Ref. 1)	4.6 (Ref. 1)	3.88	5.66	−0.300	−0.454
Xe	24.3 (Ref. 1)	4.9 (Ref. 1)	3.60	4.65	−0.175	−0.158
C_{60}	278 (Ref. 31)	13 (Ref. 3)			−0.6[f]	

[a]Values from electronic structure calculations, $\Delta V_{atop\text{-}center}$ for Ar and Xe, the magnitude of the phonon zone center gap for Kr and $\Delta V_{center\text{-}atop}$ for C_{60}.
[b]$-9V_{g0}$, where V_{g0} is the first Fourier amplitude, based on adsorbate-graphite pair potential sums, as used by McTague and Novaco (Ref. 19).
[c]$-9V_{g0}$, calculated (Ref. 49) using Carlos-Cole (CC) anisotropy terms (Ref. 50) for the potentials of Novaco and McTague, except Xe, where $V_{g0}=-6$ K$=-0.517$ meV is taken from the stability determination of Bruch and Novaco (Ref. 30).
[d]Minimum NM energy calculated with second-order perturbation theory using $V_{g0}=\Delta V/9$.
[e]Minimum NM energy calculated with second-order perturbation theory using $V_{g0}=\Delta V(\mathrm{CC})/9$.
[f]This paper, see Sec. V.

C_{60} compared to rare gases are likely to contribute to an effective flattening of the corrugation that could result in the lack of preferred orientation of the C_{60} monolayer.

Incommensurate C_{60} monolayers are rare because C_{60} chemisorbs on metal surfaces and often induces the substrate to reconstruct.[51–53] On Pb(111), C_{60} forms an apparently incommensurate monolayer (although there is some charge transfer[22] which implies chemisorption), which exhibits orientational ordering of its lattice along directions close to predictions by the NM theory.[22] This suggests that the corrugation of the C_{60}-Pb(111) potential is larger than the C_{60}-graphite potential, which is rather surprising at first glance because metals are generally considered to be "flatter" substrates for physisorbates[17] due to the smoothing effect of the conduction electrons. In fact, the corrugation experienced by some rare gases on some metal surfaces is apparently inverted relative to that expected from contours representing the surface atoms.[1,54] But based on observations for other C_{60} monolayers on metals, and on a comparison of the elastic constants of metals and C_{60}, it is unlikely that the Pb is completely unperturbed by the C_{60}, which may effectively create its own corrugation by distorting the substrate.[22] Weak C_{60} adsorption has been observed on some other surfaces, e.g., GaAs(110) (Refs. 55 and 56) and Ag/Si(111),[57] but in these cases, the C_{60} lattice is in registry with the substrate and NM epitaxial rotation does not occur.

VI. CONCLUSIONS

We have shown using LEED that submonolayer C_{60} on graphite forms incommensurate islands of close-packed C_{60} molecules having a nearest-neighbor distance that is close to the bulk value [9.99 Å compared to the 9.94 Å bulk value at 120 K (Ref. 39)] and almost random lattice orientations relative to the underlying graphite lattice. This lack of orientational order persists to subsequent layers. Our STM and LEEM studies have indicated that the C_{60} islands grow preferentially along the steps edges of the graphite, and that at step edges, the C_{60} tends to grow with close-packed rows parallel to the steps. On single-crystal graphite, this leads to the observation of a slight preference in the orientation of the C_{60} lattice along the direction 30° from the graphite lattice direction (i.e., parallel to the primary step direction).

We have used previously formulated C_{60}-C_{60} and C_{60}-graphite potentials to calculate the equilibrium epitaxial angle using the classical fully nonlinear Novaco-McTague theory. The results indicate that several angles are almost equally preferred at lattice parameters near the experimentally measured value. Since discrete angles were not observed in the experiment, we conclude that the vibrational and rotational motion of the C_{60} molecules causes an effective decrease in the C_{60}-graphite corrugation, leading to angular smearing in the observed orientations.

Since the C_{60}-graphite corrugation is effectively zero, the C_{60} represents an example of a floating solid, and therefore should be a model 2D system, albeit one with the added complexity of molecular structure. We compared the value of the thermal-expansion coefficient measured with LEED to calculated values obtained using the classical cell model using previously formulated spherically averaged C_{60} pair potentials and to values calculated using QHT with various potentials. The experimental value is about twice the expected value for a simple 2D monolayer, suggesting that either the existing models do not sufficiently take into account the vibrational and rotational degrees of freedom of the adsorbed molecules or that this layer has properties that cause it to depart from a perfectly 2D situation.

ACKNOWLEDGMENTS

We gratefully acknowledge useful conversations with Ziyou Li and John A. Venables, technical assistance from Stephanie Su, and support from Roya Maboudian for the LEEM studies. This research was supported by NSF under

Grant No. DMR-0505160. The STM work was supported through funding by the University of Virginia StartupFunding and was supported in part by the MITRE Corporation's Accelerated Graduate Degree Program (S.E.O.) (Ref. 58). The LEEM work was supported by NSF under Grant No. EEC-0832819, through the Center of Integrated Nanomechanical Systems, and by the National Center for Electron Microscopy, at Lawrence Berkeley National Laboratory, which is supported by the U.S. Department of Energy under Contract No. DE-AC02-05CH11231.

*Present address: The MITRE Corporation, McLean, VA 22102.

[1] L. W. Bruch, R. D. Diehl, and J. A. Venables, Rev. Mod. Phys. **79**, 1381 (2007).
[2] J. Götzen, D. Käfer, C. Wöll, and G. Witte, Phys. Rev. B **81**, 085440 (2010).
[3] P. A. Gravil, M. Devel, P. Lambin, X. Bouju, C. Girard, and A. A. Lucas, Phys. Rev. B **53**, 1622 (1996).
[4] R. S. Ruoff and A. P. Hickman, J. Phys. Chem. **97**, 2494 (1993).
[5] K. M. Kadish and R. S. Ruoff, *Fullerenes: Chemistry, Physics and Technology* (Wiley, New York, 2000).
[6] M. R. C. Hunt and R. E. Palmer, Surf. Rev. Lett. **3**, 937 (1996).
[7] Z. Y. Li, Surf. Sci. **441**, 366 (1999).
[8] H. Liu and P. Reinke, J. Chem. Phys. **124**, 164707 (2006).
[9] M. F. Luo, Z. Y. Li, and W. Allison, Surf. Sci. **402-404**, 437 (1998).
[10] M. F. Luo, Z. Y. Li, and W. Allison, Surf. Sci. **433-435**, 590 (1999).
[11] S. Okita and K. Miura, Nano Lett. **1**, 101 (2001).
[12] P. Reinke and P. Oelhafen, Phys. Rev. B **71**, 045420 (2005).
[13] S. Suto, A. Kasuya, C. W. Hu, A. Wawro, T. Goto, and Y. Nishina, Surf. Rev. Lett. **3**, 927 (1996).
[14] S. Suto, A. Kasuya, C. W. Hu, A. Wawro, K. Sakamoto, T. Goto, and Y. Nishina, Thin Solid Films **281**, 602 (1996).
[15] S. Szuba, R. Czajka, A. Kasuya, A. Wawro, and H. Rafii-Tabar, Appl. Surf. Sci. **144-145**, 648 (1999).
[16] H. Liu, Z. Lin, L. V. Zhigilei, and P. Reinke, J. Phys. Chem. C **112**, 4687 (2008).
[17] L. W. Bruch, M. W. Cole, and E. Zaremba, *Physical Adsorption: Forces and Phenomena* (Oxford University Press, Oxford, 1997).
[18] H. Rafii-Tabar and K. Ghafoori-Tabrizi, Prog. Surf. Sci. **67**, 217 (2001).
[19] J. P. McTague and A. D. Novaco, Phys. Rev. B **19**, 5299 (1979).
[20] A. D. Novaco and J. P. McTague, Phys. Rev. Lett. **38**, 1286 (1977).
[21] C. G. Shaw, S. C. Fain, Jr., and M. D. Chinn, Phys. Rev. Lett. **41**, 955 (1978).
[22] H. I. Li, K. J. Franke, J. I. Pascual, L. W. Bruch, and R. D. Diehl, Phys. Rev. B **80**, 085415 (2009).
[23] P. I. Cohen, J. Unguris, and M. B. Webb, Surf. Sci. **58**, 429 (1976).
[24] P. Bak, Rep. Prog. Phys. **45**, 587 (1982).
[25] N. Ferralis, K. Pussi, S. E. Finberg, J. A. Smerdon, M. Lindroos, R. McGrath, and R. D. Diehl, Phys. Rev. B **70**, 245407 (2004).
[26] K. Grzelakowski, T. Duden, E. Bauer, H. Poppa, and S. Chiang, IEEE Trans. Magn. **30**, 4500 (1994).
[27] G. S. Leatherman and R. D. Diehl, Phys. Rev. B **53**, 4939 (1996).
[28] I. Horcas, R. Fernández, J. M. Gómez-Rodríguez, J. Chochero, J. Gómez-Herrero, and A. M. Baro, Rev. Sci. Instrum. **78**, 013705 (2007).
[29] A. D. Novaco, Phys. Rev. B **22**, 1645 (1980); **19**, 6493 (1979).
[30] L. W. Bruch and A. D. Novaco, Phys. Rev. B **77**, 125435 (2008).
[31] L. A. Girifalco, J. Phys. Chem. **96**, 858 (1992).
[32] G. S. Leatherman, R. D. Diehl, M. Karimi, and G. Vidali, Phys. Rev. B **56**, 6970 (1997).
[33] S. E. O'Donnell and P. Reinke, J. Vac. Sci. Technol. B **27**, 2209 (2009).
[34] S. E. O'Donnell and P. Reinke, J. Vac. Sci. Technol. B **28**, 216 (2010).
[35] S. Morita, S. Tsukada, and N. Mikoshiba, Jpn. J. Appl. Phys., Part 2 **26**, L1511 (1987).
[36] S. Morita, S. Tsukada, and N. Mikoshiba, J. Vac. Sci. Technol. A **6**, 354 (1988).
[37] M. Sprik, A. Cheng, and M. L. Klein, J. Phys. Chem. **96**, 2027 (1992).
[38] V. K. Jindal, K. Dharamvir, and S. Singh, Int. J. Mod. Phys. B **14**, 51 (2000).
[39] K. Prassides, H. W. Kroto, R. Taylor, D. R. M. Walton, W. I. F. David, J. Tomkinson, R. C. Haddon, M. J. Rosseinsky, and D. W. Murphy, Carbon **30**, 1277 (1992).
[40] P. A. Heiney, G. B. M. Vaughan, J. E. Fischer, N. Coustel, D. E. Cox, J. R. D. Copley, D. A. Neumann, W. A. Kamitakahara, K. M. Creegan, D. M. Cox, J. P. McCauley, and A. B. Smith, Phys. Rev. B **45**, 4544 (1992).
[41] A. Pugachev, N. P. Churakova, N. I. Gorbenko, K. Saadli, and E. S. Syrkin, J. Exp. Theor. Phys. **87**, 1014 (1998).
[42] J. O. Hirschfelder, C. F. Curtiss, and R. B. Bird, *Molecular Theory of Gases and Liquids* (Wiley, New York, 1954).
[43] L. W. Bruch and J. M. Phillips, J. Phys. Chem. **86**, 1146 (1982).
[44] J. M. Phillips and L. W. Bruch, J. Chem. Phys. **79**, 6282 (1983).
[45] J. M. Pacheco and J. P. Prates Ramalho, Phys. Rev. Lett. **79**, 3873 (1997).
[46] J. Unguris, L. W. Bruch, E. R. Moog, and M. B. Webb, Surf. Sci. **87**, 415 (1979).
[47] J. Unguris, L. W. Bruch, E. R. Moog, and M. B. Webb, Surf. Sci. **109**, 522 (1981).
[48] R. D. Diehl, Ph.D. thesis, University of Washington, 1982.
[49] L. W. Bruch, in *Phase Transitions in Surface Films 2*, edited by H. Taub, G. Torzo, H. J. Lauter, and S. C. Fain (Plenum, New York, 1991), pp. 67–82.
[50] W. E. Carlos and M. W. Cole, Surf. Sci. **91**, 339 (1980).
[51] R. Felici, M. Pedio, F. Borgatti, S. Iannotta, M. Capozi, G. Ciullo, and A. Stierle, Nature Mater. **4**, 688 (2005).
[52] H. I. Li, K. Pussi, K. J. Hanna, L. L. Wang, D. D. Johnson, H. P. Cheng, H. Shin, S. Curtarolo, W. Moritz, J. A. Smerdon, R. McGrath, and R. D. Diehl, Phys. Rev. Lett. **103**, 056101 (2009).

[53] W. W. Pai and C.-L. Hsu, Phys. Rev. B **68**, 121403(R) (2003).
[54] R. D. Diehl, T. Seyller, M. Caragiu, G. S. Leatherman, N. Ferralis, K. Pussi, P. Kaukasoina, and M. Lindroos, J. Phys.: Condens. Matter **16**, S2839 (2004).
[55] Y. Z. Li, J. C. Patrin, M. Chander, J. H. Weaver, L. P. F. Chibante, and R. E. Smalley, Science **252**, 547 (1991).
[56] Y. Z. Li, M. Chander, J. C. Patrin, J. H. Weaver, L. P. F. Chibante, and R. E. Smalley, Science **253**, 429 (1991).
[57] T. Nakayama, J. Onoe, K. Takeuchi, and M. Aono, Phys. Rev. B **59**, 12627 (1999).
[58] The author's affiliation with The MITRE Corporation is provided for identification purposes only, and is not intended to convey or imply MITRE's concurrence with, or support for, the positions, opinions or viewpoints expressed by the author.